Identifying Abnormal Parathyroid Glands in the Thyroid Uptake Area Using Technetium-99m-Sestamibi and Factor Analysis of Dynamic Structures

Claire Billotey, André Aurengo, Yves Najean, Emile Sarfati, Jean-Luc Moretti, Marie-Elisabeth Toubert and Jean-Didier Rain

Service de Médecine Nucléaire et Service de Chirurgie, Hôpital Saint-Louis; Service de Médecine Nucléaire, Hôpital de la Pitié—Unité INSERM 66, Paris; and Service de Médecine Nucléaire, Hôpital Avicenne, Bobigny, France

A rapid (25 min) single tracer scintigraphic method to localize parathyroid gland abnormalities was evaluated in 24 patients with hyperparathyroidism. **Methods:** Scintigraphy was performed with ^{99m}Tc-sestamibi prior to surgery. A 25-min dynamic series centered on the neck was acquired immediately after injection of ^{99m}Tc-MIBI. Two planar static views were obtained after 1 and 2 hr. To identify abnormal parathyroid tissue in the thyroid uptake area, a factor analysis of dynamic structure (FADS) was applied to the dynamic acquisition. The results were compared to the analysis of the two planar static views. **Results:** FADS demonstrated abnormal uptake of the tracer in the thyroid area for 26 of the 31 parathyroid glands found to be abnormal at surgery (5/6 adenomas, 21/25 hyperplastic glands). In three cases, FADS demonstrated parathyroid uptake despite the absence of parathyroid tissue at surgery. FADS revealed as specific and more sensitive than the visual analysis of the two static views, since only 13/30 glands were still visible after 1 hr, and 5/26 after 2 hr. Furthermore, a study with two static views was found to be less sensitive for the detection of hyperplastic glands. **Conclusion:** FADS^{99m}Tc-MIBI is performed in less time than existing scintigraphic protocols. It is a promising method to detect abnormal parathyroid glands in the cervical area with a single tracer.

Key Words: parathyroid scintigraphy; technetium-99m-sestamibi; factor analysis of dynamic series

J Nucl Med 1994; 35:1631–1636

The use of ^{99m}Tc-MIBI or sestamibi was first proposed for parathyroid imaging in 1989 (*1*). Although one study (*2*) failed to demonstrate the superiority of this new tracer over the classic tracer, ^{201}Tl, other authors (*3–5*) have reported higher sensitivity. However, all of these methods use two tracers with the inherent disadvantages of image subtraction methods (*6–8*), although these techniques can be improved by the use of parametric methods (*9*).

Taillefer et al. (*10*) proposed a double-phase single tracer method based on the comparison of an early cervical image (10–15 min after tracer injection) and a late image (2–3 hr later). Only persistent uptake on the late image was attributed to uptake by a parathyroid gland, after O'Deherty et al. (*3*) demonstrated different kinetics of uptake and elimination of the tracer by thyroid and parathyroid tissue of adenomatous or hyperplastic glands. The thyroid gland binds the tracer more intensely, but releases it much more rapidly than abnormal parathyroid glands.

However, analysis of activity in thyroid and parathyroid regions of interest (ROIs) over time is biased when these two ROIs are superimposed. Another method of image sequence analysis that can demonstrate a difference in the kinetics of the tracer in partially superimposed regions must therefore be applied. This can theoretically be performed by factor analysis, isolating fundamental kinetics from a dynamic sequence of images (*11–15*). The starting hypothesis was that three fundamental kinetics could be identified by dynamic acquisition starting with the intravenous bolus injection of tracer: a vascular kinetic, a thyroid kinetic and a parathyroid kinetic.

If this hypothesis is accurate, factor analysis applied to early dynamic acquisition would be able to demonstrate hypertrophic cervical parathyroid glands in the thyroid area without the need for delayed images or image subtraction methods.

MATERIALS AND METHODS

Patients

We studied 24 patients (15 females and 9 males). Seven of whom had a thyroid nodule or multinodular goiter. All patients had obvious laboratory signs of hyperparathyroidism. Three types of hyperparathyroidism were observed: primary (i.e., excessive production of parathormone by mostly one or several benign adenomas, occasionally hyperplasia and rarely adenocarcinomas) in 11 patients; secondary (i.e., excessive production of parathor-

Received Nov. 4, 1993; revision accepted May 5, 1994.
For correspondence and reprints contact: Dr. Claire Billotey, Service de Médecine Nucléaire, Hôpital Saint-Louis, 1 Av Claude Vellefaux, 75010 Paris, France.

mone secondary to hypocalcemia, due to various causes, mainly chronic renal failure) in 10 patients; and tertiary (i.e., long-standing or autonomous secondary hyperparathyroidism persisting after treatment) in 3 patients. Fifteen patients had undergone resection of the abnormal parathyroid gland(s) and presented with recurrent or persistent hyperparathyroidism. The neck exploration was very recent in two patients and failed to identify all of the parathyroid anatomic abnormalities.

All but one of the patients underwent surgery 1–39 days after scintigraphy. Abnormal glands were found during surgery (38), including 31 in the neck, either ectopic or in the usual positions. We have used the common surgical mapping for parathyroid glands (*16*) i.e., L (left); R (right); P_3 (inferior); and P_4 (superior). The left superior parathyroid for example is refered to as LP_4. Histologic examination of the 31 cases with cervical abnormalities revealed 6 adenomas and 25 hyperplastic glands. The serum parathormone level correction was obtained in the dialyzed patients on the fifteenth day after surgery. In all other patients, the serum calcium returned to normal during the first 24 hr postsurgery.

One patient did not have repeat surgery, but did have negative neck exploration for recurrence of tertiary hyperparathyroidism which was performed by an experienced surgeon 1 mo before. This examination was considered to be a negative reference (Patient 21).

Data Acquisition

We used a Sopha® circular gamma camera (Gammatome 2, Sopha Medical®, Buc, France) equipped with a pinhole collimator. The zoom acquisition factor was 1.5. The patients, fasting 4 hr, were positioned (supine with head and neck extended and immobilized) so that the image field included the retromastoid region superiorly and the sternal notch inferiorly. Data acquisition was started at the time of intravenous bolus injection of 400 to 750 MBq (10 to 20 mCi) of ^{99m}Tc-MIBI (Cardiolite®, Dupont-Pharma S.A., Brussels, Belgium, Elumatic®, Oris-CEA, Gif-Sur-Yvette, France, prepared according to the manufacturer's instructions). Dynamic series of 1-min images (64 × 64 matrix) were acquired over 25 min. Figure 1 shows the eight summed images corresponding to the first 24 min of acquisition.

A second series of images were acquired: planar images of the neck and thorax with a low-energy, high-resolution, parallel-hole collimator (128 × 128 matrix—600 to 800 Kcounts) performed at 1 (20 patients) and 2 hr (17 patients).

Data processing

Factor Analysis. We applied a FADS software (Famis Software—Sopha Medical®) to the initial dynamic acquisition after temporal filtering (three-point weighted averaging). The basic principles of FADS are summarized in annex. The number of counts registered per image was 5228–172638 (median, 43089). This total count was highly dependent on the zoom factor applied to the images.

Three types of radioactivity kinetic curves in the thyroid area were identified (Figs. 2–5). The first curve corresponded to the vascular kinetic and was associated with an image of the neck vessels. The second curve was associated with a tracer elimination kinetic with a variable slope after the early uptake peak corresponded to thyroid activity. Abnormal parathyroid activity was defined by the occurrence of a nondecreasing factor kinetic after initial uptake and a related factor image exhibiting a nodular area. In one patient, operated on 24 hr before scintigraphy, the third factor was associated with a diffuse distribution in the thyroid area, probably due to the presence of local inflammation; this examination was therefore disregarded.

Double-Phase Method. Cervical uptake in the thyroid area of each late static images (1 and 2 hr scaled on the highest activity) was analyzed. A persistent uptake in the thyroid area either diffuse or limited to a portion of the thyroid (inferior or superior poles of each thyroid lobe) was considered as one (or several) abnormal parathyroid gland(s).

Data Analysis

For this study, we considered only tracer uptake projected in the thyroid area on the planar anterior view. All other uptakes, with the exception of the salivary glands, were considered to be abnormal. The 13 patients with uptake outside this area were used as negative controls of the method. Only those cases in which the site of uptake demonstrated by FADS corresponded to the anatomic site of the abnormal gland confirmed by surgery, were considered to be true-positive results. When FADS demonstrated uptake of the tracer in the thyroid area not corresponding to an abnormal parathyroid gland at surgery, results were considered to be false-positive.

The results were expressed in terms of thyroid "quadrants" (i.e., the thyroid area is divided into four parts including the upper and lower pole of each thyroid lobe, and the uptake of the tracer is analyzed in each quadrant). Tracer uptake into a large hyperplastic gland spread out across two quadrants. Results of two patients who had previous thyroid lobectomy were expressed in two quadrants. Finally, we studied tracer uptake into 88 quadrants for the FADS, 76 quadrants for DPM at 1 hr and 66 quadrants for DPM at 2 hr.

The accuracy is defined as true positive and true negative upon total number of results.

RESULTS

FADS appears to be a sensitive method (Table 1) regardless of the histologic nature of the lesion (Table 2). Figures 2–5 present the FADS results in one case of solitary parathyroid adenoma with a multinodular thyroid (Fig. 2), one case of diffuse hyperplasia (Fig. 3) and two cases of solitary hyperplastic parathyroid glands (Figs. 4 and 5) one of which had a multinodular thyroid (Fig. 5). In two cases, two abnormal images were observed, while the surgeon found only one abnormal gland. In another case, the abnormal site suggested by scintigraphy did not correspond to the anatomic site of the abnormal gland at surgery. Only four hyperplastic glands and one adenoma were not detected. These five glands were small, with a mean weight of 0.15 ± 0.056 g, while the adenoma weighed 0.080 g, statistically lower ($p < 0.02$) than the mean weight of the glands which were demonstrated by FADS (1.64 ± 2.93 g). However, very small hyperplastic glands were detected (the smallest weighing 20 mg). One of these patients in whom FADS demonstrated a false parathyroid activity had a thyroid nodule. Conversely, in two patients with a multinodular goiter and no parathyroid gland in the thyroid area, FADS only demonstrated a thyroid type of activity (i.e., the kinetic of the third factor was also decreased). Overall, FADS was found to have good accuracy.

The sensitivity of DPM was much lower than that of FADS, especially at the second hour. None of the five glands missed by FADS was visible on static films at 1 or

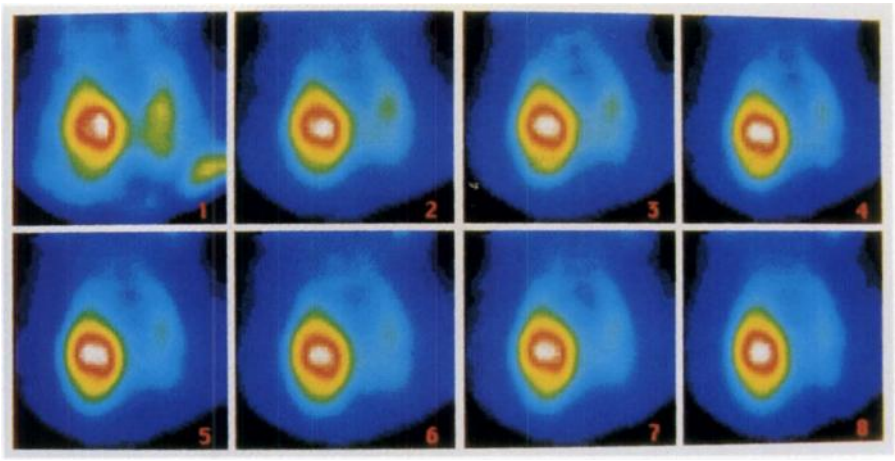

FIGURE 1. Summed images (3 min) of the first 24 min of dynamic acquisition corresponding to Patient 1. This patient suffered from primary hyperparathyroidism. The surgeon found an adenoma in the usual position of right P3 gland, weighing 13.6 g. This patient had a multinodular goiter.

2 hr. Moreover, a large number of hyperplastic glands (13/24, i.e., 13/25 in terms of thyroid quadrants at 1 hr; 19/20, i.e., 19/21 in term of thyroid quadrants at 2 hr) were no longer visible at 1 hr and especially at 2 hr (Table 2). In particular, two intrathyroid hyperplastic glands were detected by FADS, while their uptake had virtually disappeared on the 1-hr film. The much lower sensitivity of DPM was not compensated by a better specificity of this method compared to that of FADS (Table 1). DPM is therefore a less accurate method (Table 1) than FADS.

DISCUSSION

Technetium-99m-sestamibi or $^{99m}Tc(MIBI)_6$ (MIBI: 2-methoxyisobutylisonitrile) is a lipophilic cationic complex which was first proposed in 1984 as a marker of myocardial cell viability (*17*). Several studies by Chiu and Piwinica-Worms et al. (*18–20*) have demonstrated that the mechanism of uptake of Tc-sestamibi by cardiac myocytes and by fibroblasts consisted of passive distribution across plasma and mitochondrial membranes and that, at equilibrium, Tc-sestamibi is trapped within mitochondria by the large negative transmembrane potentials. Two studies have shown that 90% of the intracardiac activity of the tracer was bound to the mitochondrial fraction (*21,22*). This suggests that the higher the mitochondrial content of a cell, the more it will bind and retain this tracer. Sandrock et al. (*23*) showed that the scintigraphic detectability of abnormal parathyroid glands by ^{201}Tl was related to their large content of oxyphil cells rich in mitochondria.

Although the level of uptake of ^{99m}Tc-MIBI is lower compared to ^{201}Tl, both in abnormal parathyroid glands and in the thyroid (*3*), several studies (*3–5*) using a subtraction method have demonstrated the higher sensitivity of ^{99m}Tc-MIBI compared to ^{201}Tl, possibly because of the higher detectability of ^{99m}Tc. These physical qualities of ^{99m}Tc enable the surgeon to accurately locate hypertrophic parathyroid glands, especially mediastinal lesions on scintigraphic tomographic acquisition.

It therefore appears to be legitimate to use ^{99m}Tc-MIBI for parathyroid scintigraphy, especially as the dosimetry of this examination appears to be more favorable than for pertechnetate tracer methods and much more favorable than for ^{201}Tl methods. Indeed, considering calculations of ^{201}Tl and ^{99m}Tc-MIBI effective dose equivalent (EDE) realized by O'Deherty (*3*), choice of thyroid tracer and levels of activity used in different ^{201}Tl substraction method, the EDE is 12–28 mSv [12–26 with pertechnetate (*3,24,25*), 26–28 with ^{123}I (*3,26*)]. Comparatively, the EDE is 10 mSv for 20 mCi in our series of studies.

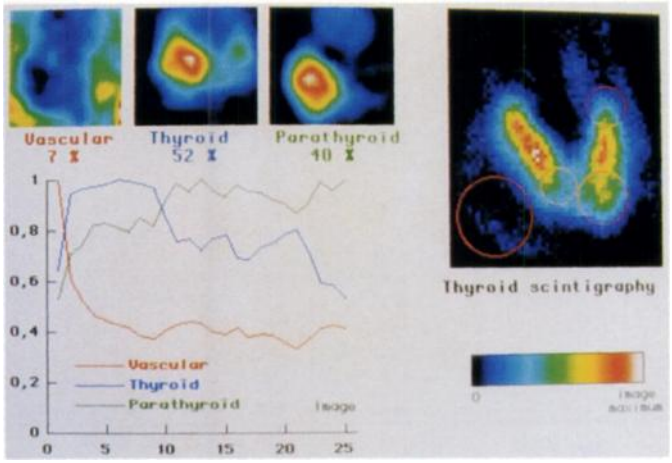

FIGURE 2. FADS results in Patient 1 (see Fig. 1). The left image is the thyroid ^{99m}Tc scintigraphy with an ROI drawn on the palpable nodules.

TABLE 1
Results of the Three Methods Expressed as Uptake in Each Thyroid Quadrant

	FADS n = 23	DPM (1 hr) n = 19	DPM (2 hr) n = 17
Sensitivity	84.5% (27/32)	55% (17/31)	23% (6/26)
Specificity	94.5% (53/56)	64.5% (29/45)	85% (34/40)
Accuracy	91% (80/88)	60.5% (46/76)	57% (40/66)

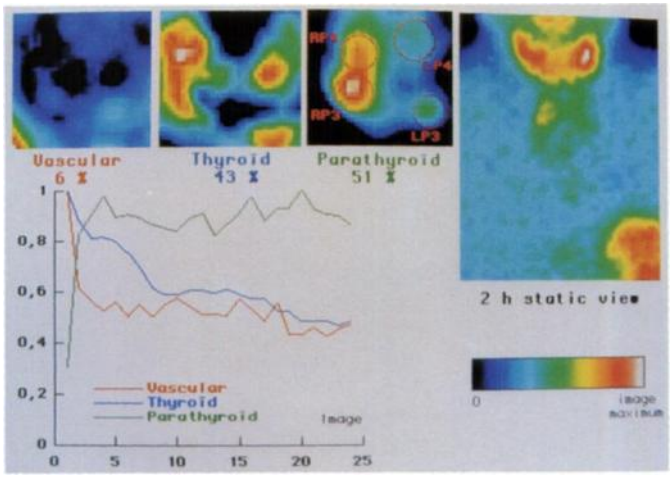

FIGURE 3. FADS results and the static view at 2 hr in a patient suffering from secondary diffuse hyperplasia. The weights of the four cervical glands found by the surgeon were: left-P3 = 1.3 g; left-P4 = 0.582 g; right-P4 = 0.137 g; and right-P3 = 1.133 g.

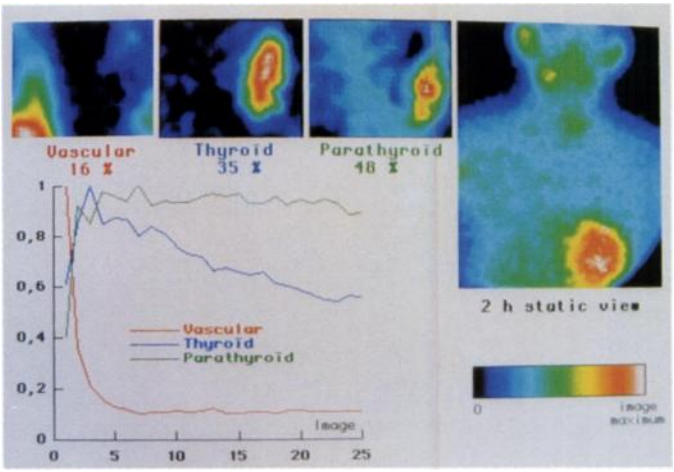

FIGURE 5. FADS results and static view at 2 hr in a patient suffering from hyperplastic primary hyperparathyroidism persisting after two previous operations (including right thyroid lobectomy). She had a polylobular and cystic, left lateroesophageal gland weighing 3 g.

Factor analysis, a method of analysis of image sequences, was introduced into nuclear medicine early in the 1970s (*27,28*). ROI analysis is an operator-dependent method and raises frequent problems of cross-talk between regions. However, whereas the factor analysis of dynamic series is able to generate more accurate curves than ROI analysis, its clinical application has remained limited.

The kinetic parameters extracted in this study appear to have a robust physiological interpretation. The types of kinetics of uptake and wash-out of ^{99m}Tc-MIBI in the thyroid and abnormal parathyroid glands demonstrated by factor analysis over the 25 min following injection of the tracer are comparable to those reported by O'Deherty et al. (*3*) i.e., virtually synchronous onset of uptake, very rapidly declining thyroid activity and persistent parathyroid activity. However, the thyroid uptake peak was often reached earlier (2 min instead of 4–6 min) and, sometimes, such as in the case of multinodular goiter, a slightly different thyroid kinetic was observed (the decline in activity was delayed by several minutes). The choice of a 25-min acquisition time was initially based on O'Deherty's results (*3*) who found the highest uptake ratio between adenomatous parathyroid tissue and thyroid tissue (in terms of activity per gram of tissue) between 15 and 25 min. Furthermore, we tried unsuccessfully to apply FADS to shorter acquisitions (particularly, small hyperplastic glands were not visible when we used an acquisition shorter than 20 min). In contrast, it could be interesting to use a 30-min acquisition in order to improve sensitivity for detecting hyperplastic glands. O'Deherty (*3*) showed that the uptake contrast between abnormal parathyroid tissue and thyroid tissue was maximal after 30 min for hyperplastic glands. In addition, this could increase the specificity of the method through a better differentiation between slow thyroid washout and nondecreasing parathyroid uptake. However, a longer exam duration increases patient movement risks and therefore must be evaluated further . A 1-min duration of each image appeared to be a good compromise between a sufficient number of images and sufficient counts per image necessary for effective FADS.

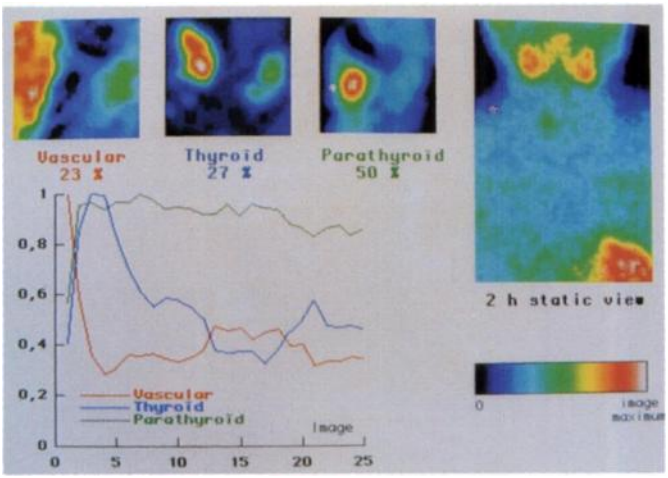

FIGURE 4. FADS results and static view at 2 hr in a patient with previous sub-total parathyroidectomy, suffering from persistent secondary hyperparathyroidism. The surgeon found a right P4 gland 1 cm in diameter inserting to the right thyroid lobe.

TABLE 2
Results Expressed as Uptake in Each Thyroid Quadrant and Respective Sensitivity of FADS and Analysis of Late Static Films According to Histology

	FADS	Static (1 hr)	Static (2 hr)
Hyperplasia	84.5% (22/26)	48% (12/25)	9.5% (2/21)
Adenomas	83.5% (5/6)	83.5% (5/6)	80% (4/5)

The results of FADS in our study cannot be strictly compared with those reported by Taillefer et al. (*10*) for the single-tracer, double-phase method for two reasons. First, this study took into account all abnormal uptakes, including those outside the thyroid area. Second, none of the patients in the Taillefer study underwent parathyroid surgery prior to scintigraphy and all but one patient presented adenomas apparently not associated with thyroid nodular disease. However, it is in this context that scintigraphy has the highest sensitivity (*3,29–32*).

The study by Liehn et al. (*9*) using subtraction methods with ^{201}Tl, appears to be fairly similar in terms of pathology distribution of the patients examined (some had secondary diffuse hyperplasia and many also had thyroid abnormalities) and especially as this study only considered areas of uptake within the thyroid area. The results of FADS appear to be comparable to the best results obtained in Liehn's study in terms of sensitivity (84.5% versus 78%) and specificity (94.5% versus 92%). In view of the modest gain in sensitivity obtained by replacing ^{201}Tl by ^{99m}Tc-MIBI in classical subtraction methods (*3–5*), comparison of a study such as Liehn's using MIBI with FADS would probably lead to the same conclusions.

CONCLUSION

The use of sestamibi for the localization of abnormal parathyroid glands in cases of recurrence or persistence of hyperparathyroidism involves an increased cost when compared to a thallium tracer. However, it provides an important gain in sensitivity which seems to justify its use. The permanent availability of this tracer constitutes an additional advantage over ^{201}Tl. FADS appears to be a good method to detect abnormal parathyroid glands in the thyroid uptake area and can replace the substraction method to avoid acquisition of a delayed view used in the single-tracer method.

ACKNOWLEDGMENTS

The authors thank Pr. G. Thomas from the statistics department (DBIM) of Saint-Louis Hospital, Paris, for statistical advice.

APPENDIX

Basic Principles of FADS

FADS is a mathematical method which enables the representation of a dynamic series of P images as a linear function of a reduced set of images and related curves referred to as factorial images (resp. curves).

From a factorial image, I and a related curve with P values, C(1), C(2) ... C(P) we define the external product E = I*f* C as a series of P images E_1, E_2 ... E_P. The image E_k is obtained by multiplying the value of each pixel of the image I by the scalar value C(k).

Let S = S_1, S_2 ... S_P be the original series of images. Its factorial decomposition is based on the estimation of R factorial images I^1 ... I^R and R related curves C^1 ... C^R which minimize the Euclidian distance between the two series:

$$S \text{ and } \sum_{r=1}^{R} I^r \otimes C^r. \qquad \text{Eq. 1}$$

For obvious physiological reasons, the factorial images and curves are bound to satisfy positivity constraints:

r each pixel of I^r has non-negative values

r each values of C^r has non-negative values

The estimation of the factorial images and curves is a three-step method:

- The goals of the first step are to reduce the amount of data and statistical fluctuations and discard insignificant pixels. To achieve this goal, the pixels are aggregated in square regions of 4 or 16 pixels. For each region, we compute the sum of the pixels in each image of the series. This yields a p-value vector refered to as a "trixel." The trixels for which the sum is lower than a predefined threshold are discarded. We usually perform a 4-pixels gathering which yields 4096 trixels in our 64 × 64 images. After region thresholding, typically 30–70 regions were retained for the next step.
- Each trixel can be represented as a point in a P-dimensional space. If the original series is actually the combination of R factorial images and curves (according to 1) the trixel points lie in an R-dimensional linear subspace and, after normalization (i.e., division of each trixel by its sum) in a (R-1) dimensional subspace. The goal of the second step is to determine this subspace. To achieve this goal, the trixels are normalized and their variance-covariance matrix is computed. The (R-1) first eigen vectors of this matrix is an orthogonal set of reference of the searched subspace. In this subspace called "factorial subspace" each point represents a P-dimensional kinetic. The points which represent non-negative kinetics are inside a polygon called "positivity area."
- The third step of FADS is devoted to factorial curves estimation. The kinetics of these curves are searched as R particular points (apex points) of the factorial subspace. To achieve the curve positivity constraints, the apex points must be inside the positivity area and to achieve the image positivity constraints, the projections of the original trixels in the factorial subspace must be inside the polyhedron of the apex points.

  The apex points estimation is done through an iterative algorithm described by Barber and improved by Bazin (*13*). After an initialization procedure (the apex is initially the R trixels with maximal mean Euclidian mutual distances), the apices are modified in order to include the original trixel projections while remaining inside the positivity area. The iterative process is stopped when stable apices are obtained (typically after about 100 iterations).
- In the last step of FADS, the kinetics of the original series are projected on the oblique reference formed by the kinetics of the apex points. The projection values on apex k constitute the factorial image k.

REFERENCES

1. Coakley AJ, Kettle AG, Wells CP, et al. Technetium-99m sestamibi—a new agent for parathyroid imaging. *Nucl Med Commun* 1989;10:791–794.
2. Ormsby PL, Jones IW, Keeling DH. Parathyroid imaging—^{201}Tl or ^{99m}Tc-sestamibi [Abstract]. *Nucl Med Commun* 1989;11:895.
3. O'Deherty MJ, Kettle AG, Wells CP, et al. Parathyroid imaging with tech-

netium 99m-sestamibi: preoperative localization and tissue uptake studies. *J Nucl Med* 1992;33:313–318.
4. Geatti O, Shapiro B, Prolo G, et al. Location of parathyroid enlargement by ^{99m}Tc-MIBI and ^{201}Tl scintigraphy, ultrasound and CT [Abstract]. *J Nucl Med* 1992;33:894.
5. Casara D, Rubello G, Saladini G, et al. Preoperative imaging of pathologic parathyroid glands (PG): comparison of ^{99m}Tc-MIBI scintigraphy, ^{201}Tl scintigraphy, neck echography (NE), computed tomography (CT) and magnetic resonance (MR) [Abstract]. *Eur J Nucl Med* 1992;19:684.
6. Ott RJ, Grey LG, Zivanovic MA, et al. The limitation of the dual radionuclide subtraction technique for the external detection of tumors by radioiodine-labelled antibodies. *Br J Radiol* 1983;56:101–108.
7. Hutton BF, Jasayinghe MAC, Bailey DL, Fulton RR. Artefact reduction in dual-radionuclide subtraction studies. *Phys Med Biol* 1987;32:477–493.
8. Perkings AC, Whalley DR, Hardy JG. Physical approach for the reduction of dual radionuclide image subtraction artifacts in immunoscintigraphy. *Nucl Med Comm* 1984;5:501–502.
9. Liehn JC, Amico S, Delisle MJ, Flement J-B. Improvement of parathyroid Tl-Tc scintigraphy using a new image subtraction method. *Eur J Nucl Med* 1981;14:184–189.
10. Taillefer R, Boucher Y, Potvin C, Lambert R. Detection and localization of parathyroid adenomas in patients with hyperparathyroidism using a single radionuclide imaging procedure with technetium-99m-sestamibi (double-phase study). *J Nucl Med* 1992;33:1801–1807.
11. Bazin JP, Di Paola R, Gibaud B, et al. Factor analysis of dynamic scintigraphic data as a modelling method. An application to the detection of metastases. In: Di Paola R, Kahn E, eds. *Information processing on medical imaging*. Paris: INSERM; 1979:345–366.
12. Barber DC. The use of principal components in the quantitative analysis of gamma camera dynamic studies. *Phys Med Biol* 1980;25:283–292.
13. Di Paola R, Bazin J-P, Aubry F, et al. Handling of dynamic sequences in nuclear medecine. *IEEE Trans Nucl Sci* 1982;29:1310–1321.
14. Aurengo A. Analyse factorielle des Sequences d'images en Médecine Nucléaire. Thèse de Doctorat d'Etat, en Sciences, Orsay, France, 1989.
15. Samal M. Factor analysis revisited: a potential key for clinicians. *Eur J Nucl Med* 1993;20:562–564.
16. Akerstrom G, Malmaeus J, Bergstrom R. Surgical anatomy of human parathyroid glands. *Surgery* 1984;95:14–21.
17. Holman BL, Jones AG, Lister-James J, et al. A new ^{99m}Tc-labeled myocardial imaging agent, hexakis (t-Butylisonitrile)-technetium (I) (Tc-99m TBI): initial experience in the human. *J Nucl Med* 1984;25:1350–1355.
18. Piwinica-Worms D, Kronauge JF, Chiu ML. Uptake and retention of hexakis (2-methoxyisobutyl isonitrile) technetium(I) in cultured chick myocardial cells, mitochondrial and plasma membrane potential dependence. *Circulation* 1990;82:1826–1838.
19. Chiu ML, Kronauge JF, Piwinica-Worms D. Effects of mitochondrial and plasma membrane potentials on accumulation of hexakis (2-methoxyisobutyl isonitrile) technetium(I) in cultured mouse fibroblasts. *J Nucl Med* 1990; 31:1646–1653.
20. Chiu ML, Herman LW, Kronauge JF, et al. Comparative effects of neutral dipolar compounds and lipophilic anions on technetium99m-hexakis (2-methoxyisobutyl isonitrile) accumulation in cultured chick ventricular myocytes. *Invest Radiol* 1992;27:1052–1058.
21. Carvalho PA, Chiu ML, Kronauge JF, et al. Subcellular distribution and analysis of technetium-99m-MIBI in isolated perfused rat hearts. *J Nucl Med* 1992;33:1516–1522.
22. Crane P, Laliberte R, Heminway S, et al. Effects of mitochondrial viability and metabolism on technetium-99m-sestamibi myocardial retention. *Eur J Nucl Med* 1993;20:20–25.
23. Sandrock D, Merino MJ, Norton JA, et al. Ultrastructural histology correlates with results of thallium-201/technetium-99m parathyroid subtraction scintigraphy. *J Nucl Med* 1993;34:24–29.
24. Ferlin G, Borsato N, Camerani M, et al. New perspectives in localizing enlarged parathyroids by technetium-thallium subtraction scan. *J Nucl Med* 1983;24:438–441.
25. Fogelman I, McKillop JH, Bessent RG, et al. Successful localisation of parathyroid adenomata by thallium-201 and technetium-99m subtraction scintigraphy: description of and improved technique. *Eur J Nucl Med* 1984; 9:545–547.
26. Neumann RD. Simultaneous dual-isotope SPECT imaging for detection and characterization of parathyroid pathology. *J Nucl Med* 1992;33:131–134.
27. Di Paola R, Penel C, Bazin JP, et al. Factor analysis and scintigraphy. In: Raynaud C, Todd-Pokropek A, eds. *Information processing in scintigraphy*. Orsay: CEA: 1976:91–123.
28. Barber DC, Duthie HL, Howlett PJ, et al. Principal components: a new approach to the analysis of gastric emptying. *Dynamic studies with radioisotopes in medicine*, 1974. Proc. Symp., Knoxville, 1974. IAEA, Vienna, 1975, 185.
29. Gooding GAW, Okerlund MD, Stark DD, et al. Parathyroid imaging: comparison of double-tracer (^{201}Tl, ^{99m}Tc) scintigraphy and high-resolution US. *Radiology* 1986;161:57–64.
30. Miller DL, Doppman JL, Shawker TH, et al. Localization of parathyroid adenomas in patients who have undergone surgery. *Radiology* 1987;162: 133–137.
31. Gimlette TMD, Brownless SM, Taylor WH, et al. Limits to parathyroid imaging with thallium-201 confirmed by tissue uptake and phantom studies. *J Nucl Med* 1986;27:1262–1265.
32. Gupta SM, Belsky JL, Spencer RP, et al. Parathyroid adenomas and hyperplasias dual radionuclides scintigraphy and bone densitometry studies. *Clin Nucl Med* 1985;10:243–245.